LANGMUIR

pubs.acs.org/Langmuir Article

Hydrodynamic–Colloidal Interactions of an Oil Droplet and a Membrane Surface

Mariano Galvagno and Guy Z. Ramon*

Cite This: https://dx.doi.org/10.1021/acs.langmuir.9b03778 Read Online

ACCESS | Metrics & More | Article Recommendations

ABSTRACT: Membranes have been shown to be exceptionally successful in the challenging separation of stable oil/water emulsions but suffer from severe fouling that limits their performance. Understanding the mechanisms leading to oil deposition on the membrane surface, as influenced by hydrodynamics and colloidal surface interactions, is imperative for informing better engineered membrane surfaces and process conditions. Here, we study the interactions between an oil droplet and a membrane surface. Hydrodynamics within the water film, confined between the droplet and the membrane, are captured within the framework of the lubrication approximation, coupled with the van der Waals (vdW) and electrostatic interactions through the droplet shape, which is governed by an augmented Young–Laplace equation. The model is used to calculate possible equilibrium positions, where the droplet is held at a finite distance from the membrane by a balance of the forces present. An equilibrium phase diagram is constructed as a function of various process parameters and is shown in terms of the scaled permeation rate through the membrane. The phase diagram identifies the range of conditions leading to deposition, characterized by a "critical" permeation rate, beyond which no equilibrium exists. When equilibrium positions are permitted, we find that these may be classified as stable/unstable, in the kinetic sense. Further, our results demonstrate the link between the deformation of the droplet and the stability of equilibria. An upward deflection of the droplet surface, owing to a dominant, long-range repulsion, has a stabilizing effect, as it maintains the separation between the droplet and membrane. Conversely, a downward deflection is destabilizing because of the self-amplifying effect of strongly increasing attractive forces with separation distance—as the surfaces are pulled together because of deformation, the attractive force increases, causing further deformation. This is also manifested by a dependence of the bistable region on the deformability of the droplet, which is represented by a capillary number, modified so as to account for the effect of the permeable boundary. As the droplet becomes more easy to deform, the transition from an unconditionally stable region of the phase diagram to a point beyond which there is no equilibrium (interpreted as deposition) becomes abrupt. These results provide valuable physical insights into the mechanisms that govern oil fouling of membrane surfaces.

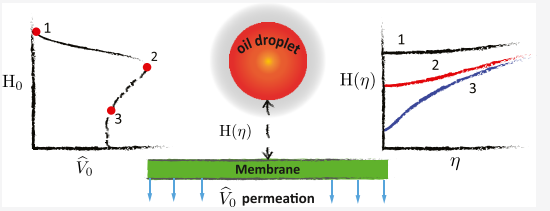

INTRODUCTION

The separation of stabilized oil-in-water emulsions poses a difficult technological challenge, often with important environmental implications. This is particularly so when treating oily wastewater from various industries, including oil and gas production, prior to discharge so as to minimize pollution and contamination of freshwater sources and the marine environment.[1,2] Current treatment methods include flotation, coagulation, biological treatment, membrane separation technology, advanced oxidation processes, and combined technologies.[3,4] In particular, membranes have been successful in effectively separating stable emulsions of oil droplets (<20 μm in diameter), difficult to achieve by other techniques.[4,5] While exceptionally successful at performing the actual separation, membranes suffer from severe fouling due to oil deposition during operation, which results in loss of productivity and requires extensive back-washing and cleaning that can considerably increase costs.

Fouling is a long-standing issue in membrane separation, particularly when colloidal material is involved. In many cases, understanding the characteristics of the specific process, namely, the separated mixture, membrane used, and operating conditions—particularly the permeation flux through the membrane—can be used to identify a "critical flux", below which fouling is minimized.[6] The main idea behind this concept is that the primary cause of colloidal deposition is the permeation through the membrane, so that if some repulsive forces are present, choosing the right permeation rate can reduce deposition significantly. Furthermore, in certain cases, deposition has been shown to be reversible—a particle seemingly deposited at the membrane surface is released upon shutting off the permeation.[7] Understanding the

Received: December 9, 2019
Revised: February 25, 2020
Published: February 26, 2020

influence of the hydrodynamic force due to permeation and how it balances against surface interactions (such as electrostatic repulsion) between colloidal particles and membranes will allow for better design of membrane materials and process conditions; this is particularly so for emulsions, where micron-scale droplets are involved. Although there has been much work devoted to modifying the membrane surface, imparting antifouling properties,[8] there is still insufficient mechanistic understanding of oil droplet deposition and how this is affected by droplet deformation.

Recent experimental work has begun to provide insight into droplet behavior at the membrane surface, using microscopic observation.[9−13] These have shown various aspects such as droplet accumulation, coalescence, and release. In particular, it has been shown that there is a link between droplet deformation, as measured using confocal microscopy imaging analysis, and the reversibility of deposition—droplets that retained a near-spherical shape were easily washed off the membrane upon shutting off of the permeation, whereas deformed droplets remained attached.[10]

The hydrodynamic interaction between a rigid sphere and a permeable wall has been theoretically studied quite extensively (the interested reader may find many of these studies summarized in ref 14). In particular, the increased viscous drag induced by the proximity to a permeable boundary has been studied in the context of the low permeabilities and colloidal particle sizes representative of commercial membrane separations[15] and also considered the effect of shape and of the possible existence of equilibrium positions at a finite distance from the membrane surface.[14] While providing important insight, however, these studies all consider rigid, non-deformable particles.

Herein, we study the case of a single droplet in equilibrium, at close proximity to a filtration membrane through which the surrounding fluid flows. Specifically, a mathematical model is derived, capturing the interplay between droplet deformation and the resultant forces acting on the droplet due to hydrodynamic and colloidal surface interactions—incorporated via a disjoining pressure. The model is then used to identify the existence of equilibrium positions of the droplet at a finite distance from the membrane surface, the stability of equilibria and dependence on droplet shape and the various parameters involved.

PROBLEM FORMULATION

Geometry and Long-Wavelength Approximation. We consider an initially spherical oil droplet, with radius R, immersed in an incompressible Newtonian fluid, at close proximity to a permeable surface through which a flow is driven (see Figure 1 for a schematic illustration of the system). The permeable surface (a separation membrane) is assumed to have a uniform permeance (permeability per unit thickness) k, and V_0 represents the uniform permeation rate through the membrane, in the absence of the droplet.

The equations of motion and continuity of the fluid confined within the gap between the approaching droplet and the membrane surface can be significantly simplified by invoking the lubrication approximation, valid when $h \ll R$.[16] Furthermore, we assume that the interface is immobile, corresponding with either a very large viscosity ratio or the presence of a sufficient amount of surfactant molecules;[17] this results in an imposed no-slip condition and a situation where the flow inside the droplet may be ignored. Under these

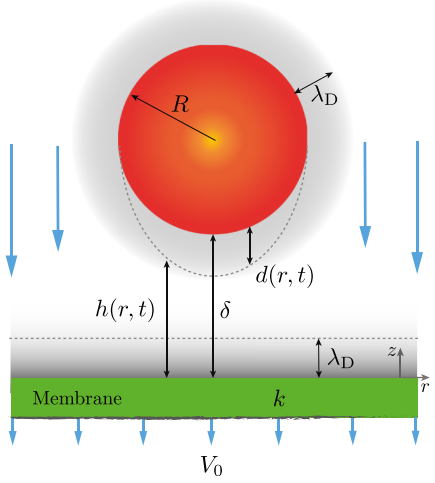

Figure 1. Schematic illustration of a liquid droplet with radius R, immersed in a second, immiscible liquid close to a membrane with permeance (permeability per unit thickness) k. $h(r,t) \simeq \delta + r^2/2R + d$ is the thickness of the layer confined between the droplet and the membrane, in which the droplet deformation is $d(r,t)$ and δ is the distance of closest approach between an undeformed droplet and the membrane (note that the deformation is shown to be negative in the sketch, but can be positive as well). The permeation velocity through the membrane is V_0 and λ_D is the Debye length.

assumptions, and accounting for the permeation through the boundary, we may write the equation for the pressure within the thin fluid film, separating the droplet and the membrane, as[14,15]

$$\frac{\partial h}{\partial t} = \frac{1}{12\mu r}\frac{\partial}{\partial r}\left(rh^3\frac{\partial p}{\partial r}\right) - \frac{k}{\mu}p - V_0, \tag{1}$$

where μ is the fluid viscosity and p is the hydrodynamic pressure. This equation describes the deviation of the pressure from the far-field, background pressure away from the drop (see refs 14 and 15 for further details of this derivation). The shape of the droplet near the apex is governed by the linearized, augmented Young−Laplace equation, representing the normal stress balance at the interface[18]

$$\frac{\sigma}{r}\frac{\partial}{\partial r}\left(r\frac{\partial h}{\partial r}\right) = \frac{2\sigma}{R} - \mathcal{P}(r, t). \tag{2}$$

Here, σ is the surface tension coefficient and $\mathcal{P}$ is the generalized stress, defined as

$$\mathcal{P}(r, t) = p + \Pi(h), \tag{3}$$

which includes the hydrodynamic pressure $p(r,t)$ and the additional stresses, $\Pi(h)$, resulting from surface interactions (disjoining pressure); here, these are taken as the simple sum of an attractive van der Waals (vdW) stress accounting for the wettability and a repulsive electrostatic stress[19]

$$\Pi(h) = -\frac{A_H}{6\pi h^3} + \zeta\, e^{-h/\lambda_D}, \tag{4}$$

in which A_H is the Hamaker constant, λ_D is the Debye length, representing the characteristic decay length of electrostatic repulsion, and ζ is a parameter characterizing the electrostatic interaction (or electrostatic stress at contact)[19]

https://dx.doi.org/10.1021/acs.langmuir.9b03778
Langmuir XXXX, XXX, XXX−XXX

Table 1. Orders of Magnitude for Dimensional Parameters of the Problem

parameter	description	parameter	description
$A_H \approx 10^{-21}$ J	Hamaker constant	$R \approx 10^{-7}$ to 10^{-5} m	droplet radius
$\zeta \approx 10^{4}$ Pa	electrostatic stress at contact	$\mu \approx 10^{-3}$ Pa s	viscosity
$\lambda_D \approx 10^{-9}$ to 10^{-7} m	Debye length	$V_0 \approx 10^{-5}$ to 10^{-4} m/s	permeation velocity
$\delta \approx 10^{-8}$ m	distance to the membrane	$k \approx 10^{-13}$ to 10^{-12} m	membrane permeance
$\sigma \approx 10^{-2}$ N/m	surface tension	$l_H = 10^{-10}$ to 10^{-8} m	hydrodynamic decay length

$$\zeta = 64k_bTc_\infty \tanh\left(\frac{ze\psi_p}{4k_bT}\right)\tanh\left(\frac{ze\psi_m}{4k_bT}\right), \tag{5}$$

where k_b is the Boltzmann constant, c_∞ denotes the background electrolyte concentration, z the ion valency, T the absolute temperature, e corresponds to the elementary charge, and ψ is the electric "zeta" potential, with subscripts p and m denoting particle and membrane, respectively. We note that the choice made here with respect to the colloidal interactions is by no means comprehensive and mostly serves as an illustrative example of the possible framework offered by the model. For example, more elaborate forms of the electrostatic stress may be used, as well as other forms of the vdW interaction (e.g., including retardation effects as well as a positive Hamaker constant[19,20]). Certainly, one may prescribe other forms of the disjoining pressure that include structural and solvation interactions, and so forth.

The primary goal of the current study is to examine the stationary droplet, that is, the case of a droplet at equilibrium. Under such conditions, the net force acting on the droplet must vanish and is imposed as an integral constraint

$$\sum F = \int_0^\infty r\mathcal{P}(r, t)\mathrm{d}r = 0. \tag{6}$$

Note that the long-wavelength model formulation focuses on the region of the droplet closest to the membrane, specifically on the gap between the membrane and the droplet—the lubrication area—where the hydrodynamic stresses originate. The force calculated from integration of the hydrodynamic stresses does not include the usual "Stokes drag" acting on the entire drop, which has been shown to be much smaller (up to 2−4 orders of magnitude).[15] We also neglect the effect of deformation on the entire drop, assuming that it is confined to a region on the order of $(Rh)^{1/2}$ (for a more detailed view on how stresses change due to whole droplet deformation see refs 20 and 21).

Scaled, Steady-State Equation. To study droplets at equilibrium, we solve the steady-state version of eq 1 by setting $\partial h/\partial t = 0$. Equations 1 and 2 are nondimensionalized by scaling the hydrodynamic pressure using a modified viscous stress, $p = (\mu V_0/k)P$, that also incorporates the permeance of the membrane as a length scale. Through inspection, balancing the remaining terms in the equations requires the scaling for the radial coordinate r and gap width h to be $r = \eta(96kR^3)^{1/4}$ and $h = H(24kR)^{1/2}$, respectively. Using these scaling transformations, we have the steady-state dimensionless equations for the gap width $H(\eta)$ and hydrodynamic pressure $P(\eta)$

$$\frac{1}{\eta}\frac{\partial}{\partial\eta}\left(\eta H^3\frac{\partial P}{\partial\eta}\right) - P + 1 = 0, \tag{7}$$

and the scaled Young−Laplace equation

$$\frac{1}{2\eta}\frac{\partial}{\partial\eta}\left(\eta\frac{\partial H}{\partial\eta}\right) - 2 + \widehat{Ca}\left(P + \frac{1}{\widehat{V}_0}\widetilde{\Pi}\right) = 0. \tag{8}$$

Here, as we are also interested in the droplet deformation, we define the gap width as $H = \hat{\delta} + \eta^2 + \hat{d}$. The deflection $\hat{d}(\eta)$, and $\hat{\delta}$, the distance of closest approach to the membrane of an undeformed droplet are scaled against the hydrodynamic decay length $l_H = (24kR)^{1/2}$. The term η^2 comes from the parabolic approximation of the unperturbed, spherical droplet shape. Recasting the steady-state equations in terms of the deflection yields the system

$$\frac{1}{\eta}\frac{\partial}{\partial\eta}\left[\eta(\hat{\delta} + \eta^2 + \hat{d})^3\frac{\partial P}{\partial\eta}\right] - P + 1 = 0, \tag{9}$$

$$\frac{1}{\eta}\frac{\partial}{\partial\eta}\left(\eta\frac{\partial\hat{d}}{\partial\eta}\right) + 2\widehat{Ca}\left(P + \frac{1}{\widehat{V}_0}\widetilde{\Pi}\right) = 0, \tag{10}$$

and the scaled equilibrium condition

$$\hat{F} = \int_0^\infty \eta\left(P + \frac{1}{\widehat{V}_0}\widetilde{\Pi}\right)\mathrm{d}\eta = 0. \tag{11}$$

The scaled equations contain several dimensionless parameters. First, $\widehat{Ca} = \mu V_0 R/\sigma k$ is a modified capillary number, accounting for the ratio of the viscous and the surface tension stresses and differing from the classical capillary number by the factor R/k, which comes from the hydrodynamic interaction with the permeable boundary. Next, the scaled permeation $\widehat{V}_0 = \mu V_0/k\zeta$ represents the ratio of the viscous and repulsive electrostatic stresses at contact. Finally, $\widetilde{\Pi}$ is the nondimensional disjoining pressure defined as

$$\widetilde{\Pi}(H) = -\frac{\widehat{A}_H}{H^3} + \mathrm{e}^{-H/\hat{\lambda}_D} \tag{12}$$

with $\widehat{A}_H = A_H/6\pi\zeta l_H^3$ the scaled Hamaker constant, accounting for the ratio of attraction and repulsion stresses and $\hat{\lambda}_D = \lambda_D/l_H$ is the ratio of the electrostatic and the hydrodynamic decay lengths. Typical physical values and ranges of process parameters are shown in Table 1, whereas in Table 2 we summarize all of the nondimensional parameters and corresponding orders of magnitudes used in the forthcoming analysis.

Finally, we specify the boundary conditions imposed on the system of equations. At the origin, $\eta = 0$, we have symmetry considerations, that is

$$\frac{\partial\hat{d}}{\partial\eta} = 0,$$
$$\frac{\partial P}{\partial\eta} = 0. \tag{13}$$

https://dx.doi.org/10.1021/acs.langmuir.9b03778
Langmuir XXXX, XXX, XXX−XXX

Table 2. Definition of Nondimensional Parameters, Characteristic Ranges of Orders of Magnitude, and Description

nondimensional parameters	characteristic ranges	description
$\widehat{V}_0 = \mu V_0/k\zeta$	10^{-4} to 10^{4}	ratio of viscous-repulsive stresses
$\widehat{Ca} = \mu V_0 R/\sigma k$	0−100	ratio of viscous-surface tension stresses
$\hat{\lambda}_D = \lambda_D/l_H$	1−100	ratio of electrostatic-hydrodynamic decay length scales
$\widehat{A}_H = A_H/6\pi\zeta l_H{}^3$	10^{-3} to 1	scaled colloidal stress
$\hat{\delta} = \delta/l_H$	10^{-5} to 10^{3}	scaled distance of closest approach
$l_H = (24kR)^{1/2}$	10^{-10} to 10^{-8} m	hydrodynamic decay length

Far from the apex, we expect the pressure to decay back to the background value, and the deflection to likewise vanish[18,22,23] as $\eta \to \infty$, which for the numerical scheme corresponds to the simulation domain $\eta = L$, so we impose

$$\hat{d} = 0, \qquad \frac{\partial P}{\partial \eta} + 4\frac{P}{\eta} = 0. \tag{14}$$

RESULTS AND DISCUSSION

In order to obtain the droplet shape and pressure profiles at equilibrium, where the droplet is stationary and under a zero net force, we solve the second-order problem given by eqs 9−11 along with the boundary conditions presented in eqs 13 and 14. The system is solved numerically using the AUTO 07p continuation package,[24,25] for parameter ranges described in Table 2. For all numerical calculations, the domain size is set to $L = 10$, which was found adequate in assuring that the pressure and deformation decay to zero in the far-field, independent of the choice of the domain size.

Equilibrium Phase Diagram. The main outputs of these calculations are the distributions of the various stress components, in particular the hydrodynamic pressure, as well as the shape of the droplet. However, an even more interesting outcome is the very existence of a solution for which an equilibrium exists and $(H > 0)$; beyond a particular region of parameter space, no such equilibrium exists. We further find that, for a certain range of parameters, two solutions exist. This behavior was previously described by Ramon et al.[14] for rigid spherical particles but is here modified by the deformation of the droplet shape and the inclusion of the vdW force.

The measure used to construct the phase diagrams is the distance between the droplet and the membrane at the origin, $H_0 \equiv H(0) = \hat{\delta} + \hat{d}(0)$, plotted against the scaled permeation, $\widehat{V}_0 \equiv \mu V_0/k\zeta$, which represents a main feature of the current problem—the permeable boundary, a defining characteristic of the separation membrane (see Figure 2a for an example of the phase diagram and its general features). When a finite distance separates the droplet from the membrane under equilibrium, it means that adhesion may be prevented by repulsive forces. This distance would be smaller or larger than that obtained for a rigid particle, dependent on whether there is a downward or upward deflection of the droplet surface, respectively. When no equilibrium solution exists we interpret this as deposition—the droplet makes contact with the surface. Finally, when two

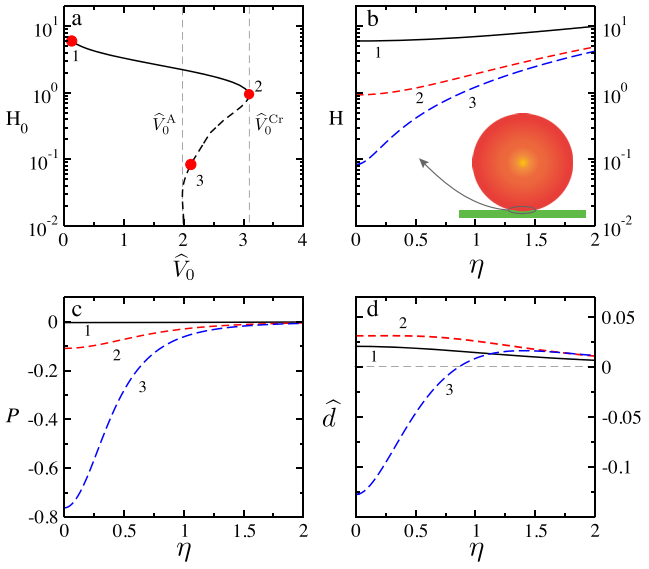

Figure 2. Pressure and droplet profiles for different values of modified permeation $\widehat{V}_0$. Panel (a) shows H_0 as a function of the modified permeation $\widehat{V}_0$ for $\widehat{A}_H = 0.001$, $\hat{\lambda}_D = 1$, and $\widehat{Ca} = 1$. Labels correspond to droplet profiles, pressure distribution, and deflection profiles shown in subsequent panels. Dashed black line corresponds to unstable solutions branch. Panel (b) shows droplet profiles for different values of $\widehat{V}_0$ as indicated. The inset indicates the region of interest. Panels (c,d) depict pressure distribution and deflection profiles respectively.

solutions exist, one solution is understood to be stable, at least in the kinetic sense, whereas the other is unstable. Kinetic stability refers, here as in the classical sense, to the existence of an energy barrier in the presence of Brownian motion; even if the force balance predicts an equilibrium position, there may still be a thermal "kick" large enough to overcome the energy barrier and cause the surfaces to make contact. We note that the calculation of the energy barrier and, hence, a measure of the actual kinetic stability and its characteristic time-scale, requires the solution of the full transient problem and is beyond the scope of the present study. The point of vanishing stable solutions is also where the unstable branch emerges. On a plot of H_0 versus $\widehat{V}_0$, this point (marked as point 2 on Figure 2a) embodies the existence of the "critical flux", $\widehat{V}_0^{Cr}$, for a given membrane−emulsion system, as beyond this point deposition will always occur. Because $\widehat{V}_0$ represents the operating permeation rate and properties of the emulsion, it allows a choice of operating conditions to shift the system from regions of rapid deposition to regions of delayed deposition.

Droplet Profiles at Equi-Valued Scaled Permeation. Interesting features that accompany the equilibrium solution are the trends in the distributions of the pressure and deflection, as well as the overall droplet shape near the origin. In order to further understand this behavior, we examine the case of solutions found for an equal value of the scaled permeation rate, $\widehat{V}_0 \approx 2$, and their differences. Following the inset of Figure 3a, points 1−3 marked on the phase diagram signify, on each of the subsequent plots, stable versus unstable deflections (a) and their corresponding generalized stress (b), colloidal stress, (c) and hydrodynamic stress (d) profiles. Stable solutions are seen to be upward-deflecting, meaning that repulsion is significant enough to push the droplet surface away from the membrane surface, resulting in a stable solution—no

https://dx.doi.org/10.1021/acs.langmuir.9b03778
Langmuir XXXX, XXX, XXX−XXX

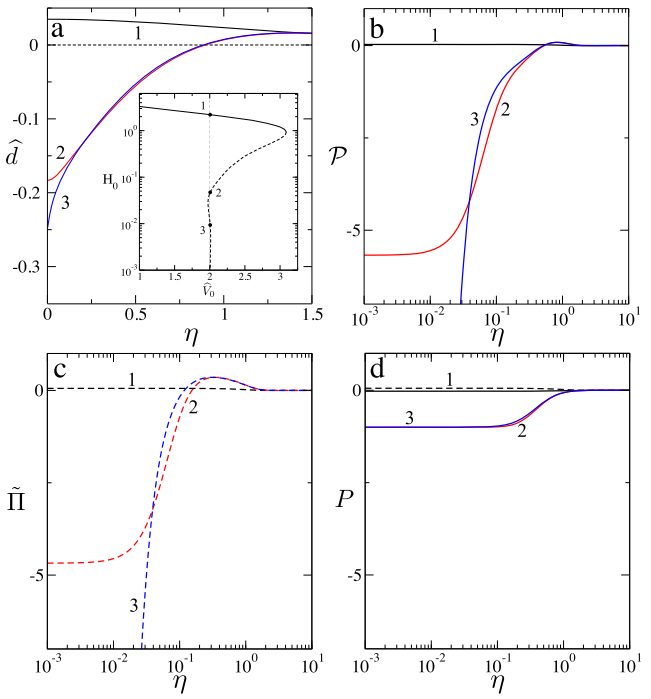

Figure 3. Deflection and stress profiles for solutions to equal-values scaled permeation $\widehat{V}_0 \approx 2$, for $\widehat{A}_H = 0.001$, $\hat{\lambda}_D = 1$, $\widehat{Ca} = 1$, corresponding with the phase diagram shown in the inset of panel (a), in which labels 1−3 correspond to profiles shown in subsequent panels. (a) Deflection profiles $\hat{d}$, note the steepness of the deflection in profile (3). (b) Generalized stress $\mathcal{P}$. (c) Colloidal stress $\tilde{\Pi}$. (d) Hydrodynamic stress P.

adhesion. Conversely, unstable solutions are seen to be downward-deflected, which reduces the gap between the droplet and membrane surfaces compared with the equivalent, rigid case. The reason behind the unstable nature of this solution lies in the physics of the hydrodynamic interaction, which is the main attractive force acting on the droplet at longer ranges. This interaction increases as the separation distance decreases, so a downward-deflection is a self-amplifying mechanism—the permeation decreases the pressure in the confined gap between the two surfaces, which causes the downward deflection, which further decreases the pressure and so on. The scales for both the hydrodynamic stress and the scaled colloidal stress show that the attractive colloidal stress component becomes stronger than the electrostatic repulsion as the droplet apex gets closer to the membrane and thus increases the negative deflection. This presumably promotes the irreversible deposition of the droplet on the membrane. The case examined shows the existence of a stable profile (1) and two unstable profiles (2) and (3) for the same modified permeation $\widehat{V}_0$. Therefore, we find that, compared with the behavior of a rigid particle, deformability can have a stabilizing effect, but then also exhibits a more abrupt transition. The cusping is due to vdW attraction, that become dominant at close proximity and eventually induces a profile reminiscent of "pinch-off" at the droplet leading edge.

Influence of Process Parameters on Equilibria and the "Critical Flux". The influence of the various parameters characterizing the process is illustrated in Figure 4. Specifically, the deformability of the droplet is governed by the modified capillary number $\widehat{Ca}$, representing the ratio of viscous forces tending to deform the droplet and surface tension that tends to

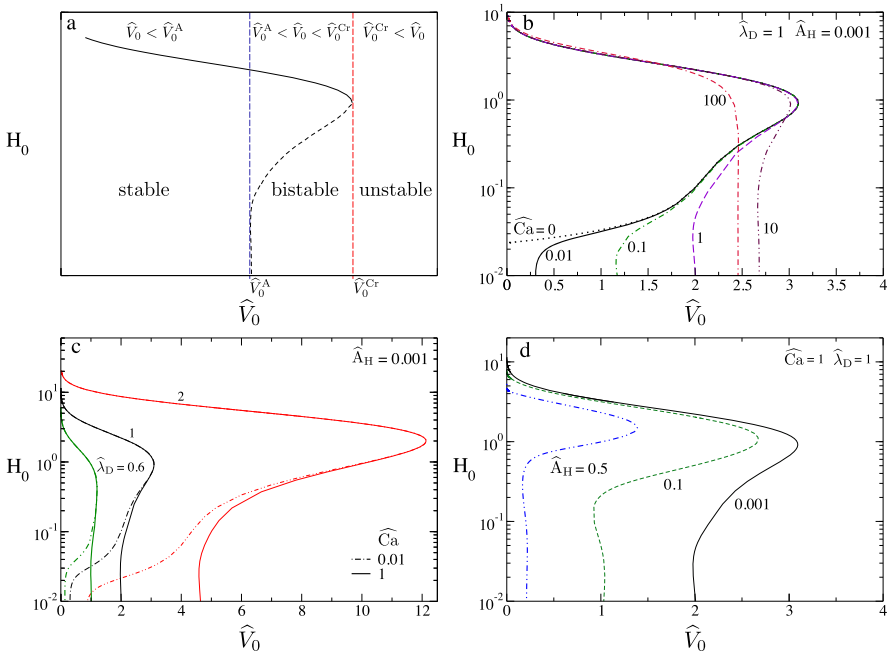

Figure 4. (a) Sketch of the equilibrium phase diagram, identifying the critical scaled permeation $\hat{V}_0^{Cr}$ (where $\widehat{V}_0 = \mu R V_0 / k\zeta$) and the detachment permeation $\hat{V}_0^{A}$, as well as different stability regions. Upper branch correspond to stable solutions (solid black line) and lower branch to unstable solutions (dashed line). (b) Gap width at the origin H_0 as a function of the scaled permeation $\widehat{V}_0$ for different values of the modified capillary number $\widehat{Ca} \equiv \mu V R / \sigma k$. The scaled Debye length $\hat{\lambda}_D = 1$ and Hamaker constant $\widehat{A}_H = 0.001$. (c) H_0 vs $\widehat{V}_0$ for different values of the modified capillary number $\widehat{Ca}$ and scaled Debye length $\hat{\lambda}_D$. (d) H_0 vs $\widehat{V}_0$ for different values of the scaled Hamaker constant $\widehat{A}_H = 0.001$, 0.1 and 0.5.

https://dx.doi.org/10.1021/acs.langmuir.9b03778
Langmuir XXXX, XXX, XXX−XXX

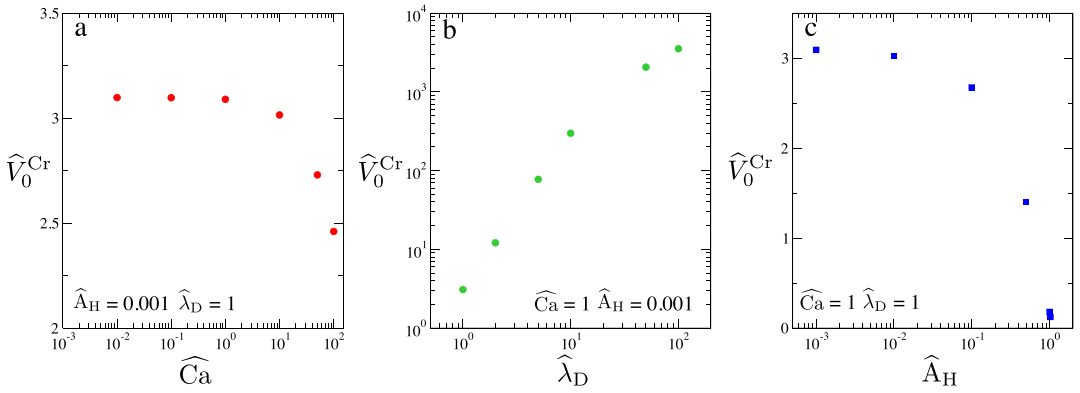

Figure 5. Critical permeation flux for different process parameters: the panels depict how the critical permeation flux $\widehat{V}_0^{Cr}$ change for different values of process parameters: $\widehat{Ca}$ (panel (a)), $\widehat{\lambda}_D$ (panel (b)) and $\widehat{A}_H$ (panel (c)) as shown.

retain the spherical shape (see e.g. ref 23); the scaled Debye length $\widehat{\lambda}_D$ represents the ratio of electrostatic−hydrodynamic decay lengths and hence their relative dominance at long-range; finally, the scaled Hamaker constant $\widehat{A}_H$ indicates the ratio of attractive−repulsive colloidal stresses considered in the current problem. A sketch of the equilibrium phase diagram and corresponding equilibria regions is presented in Figure 4a, separating regions of stable and unstable parameter space. As already mentioned earlier, for a given set of parameters, there is a value of $\widehat{V}_0$ above which no equilibrium exists and this is interpreted as deposition of the droplet onto the membrane, occurring beyond a "critical" permeation ($\hat{V}_0^{Cr}$). However, we also distinguish between two regions that do permit equilibria—one region in which both a stable and an unstable solution exist (for $\hat{V}_0^{A} < \widehat{V}_0 < \hat{V}_0^{Cr}$, where we define $\hat{V}_0^{A}$ as the point where the unstable branch corresponds with "pinch-off" of the droplet leading edge) and another which is unconditionally stable. The latter appears to be the consequence of the droplet deformability, as shown in Figure 4b. For a rigid particle ($\widehat{Ca} = 0$), in the presence of vdW attraction, such an unconditionally stable region does not exist. However, we see that as $\widehat{Ca}$ increases, indicating a stronger tendency of the droplet to deform, two things occur: First, the unconditionally stable region is pushed to higher permeation rates. This is presumably the consequence of strongly repulsive conditions, under which the droplet experiences an upward deflection and does not make contact with the membrane, and this tendency increases as it becomes easier to deform the droplet. The second noticeable effect is that the bistable region becomes smaller, not only because of the stabilizing effect of deformation, but also, at large enough $\widehat{Ca}$, because the "critical flux" is decreased—and so deformation becomes de-stabilizing.

A reduction of $\hat{V}_0^{Cr}$ also occurs when the scaled Debye length is decreased (see Figure 4c), which results in a shorter-ranged electrostatic repulsion, compared with the attractive force resulting from the hydrodynamic interaction. Similarly, and as can be expected, a larger scaled Hamaker constant likewise decreases the critical scaled flux (see Figure 4d).

The overall trend observed for the critical scaled flux, $\hat{V}_0^{Cr}$, is shown as a function of the various process parameters in Figure 5. Increasing the capillary number $\widehat{Ca}$ leads to smaller $\widehat{V}_0^{Cr}$ and abrupter transition value (a), a larger modified Debye length $\widehat{\lambda}_D$ increases the critical flux (b) and larger values of the scaled colloidal stress $\widehat{A}_H$ decrease the critical flux.

CONCLUSIONS AND OUTLOOK

Understanding the interaction of droplets with the surface of separation membranes is crucial for developing better materials and improved process conditions aimed at reducing or reversing fouling during oil/water emulsion separation. With the use of a hydrodynamic model, coupled with the equation governing the droplet shape, and incorporating colloidal attractive and repulsive stresses, we have shown the existence of different equilibria regions: stable, bistable, and unstable. These have implications toward regimes under which deposition always occurs, versus conditions which may reduce the rate of deposition, or possibly increase its reversibility. The stability threshold is given by a "critical" scaled permeation $\widehat{V}_0^{Cr}$ for which, at larger values of $\widehat{V}_0$, a stable equilibrium ceases to exist. An equilibrium phase diagram was constructed in terms of different process parameters, reflecting the relative importance of hydrodynamic and colloidal stresses, both in terms of their magnitude but also in terms of their range. Within the phase diagram, stable and unstable droplet shapes are identified. Stable droplet shapes feature upward deflection, due to the prevalence of long-range repulsion—increasing the electrostatic decay length $\hat{\lambda}_D$ results in an increased critical flux $\widehat{V}_0^{Cr}$. Increasing the modified capillary number $\widehat{Ca}$, representing a more easily deformable droplet, is a primary reason for an increased stable region owing to an upward deflection, but will eventually lead to a lower critical flux and an abrupt transition leading to deposition. The scaled colloidal stress $\widehat{A}_H$ in turn decreases the critical permeation, making the system less stable. Future possible directions stemming from this work are the extension of the model to allow droplet spreading and identifying final shape-contact area, as well as calculating energy barriers from dynamical simulations.

AUTHOR INFORMATION

Corresponding Author

Guy Z. Ramon − *Department of Civil & Environmental Engineering, Technion - Israel Institute of Technology, Haifa 3200003, Israel;* orcid.org/0000-0002-0711-0654; Email: ramong@technion.ac.il

https://dx.doi.org/10.1021/acs.langmuir.9b03778
Langmuir XXXX, XXX, XXX−XXX

Author

Mariano Galvagno − *Department of Civil & Environmental Engineering, Technion - Israel Institute of Technology, Haifa 3200003, Israel*

Complete contact information is available at: https://pubs.acs.org/10.1021/acs.langmuir.9b03778

Notes

The authors declare no competing financial interest.

■ ACKNOWLEDGMENTS

The research was funded by the Israel Science Foundation (ISF) grant number 2018/17. M.G. was supported in part by a fellowship from the Lady Davis Foundation at the Technion.

■ REFERENCES

(1) Mondal, S.; Wickramasinghe, S. R. Produced water treatment by nanofiltration and reverse osmosis membranes. *J. Membr. Sci.* **2008**, *322*, 162−170.

(2) Vengosh, A.; Jackson, R. B.; Warner, N.; Darrah, T. H.; Kondash, A. A Critical Review of the Risks to Water Resources from Unconventional Shale Gas Development and Hydraulic Fracturing in the United States. *Environ. Sci. Technol.* **2014**, *48*, 8334−8348.

(3) Fakhru'l-Razi, A.; Pendashteh, A.; Abdullah, L. C.; Biak, D. R. A.; Madaeni, S. S.; Abidin, Z. Z. Review of technologies for oil and gas produced water treatment. *J. Hazard. Mater.* **2009**, *170*, 530−551.

(4) Shaffer, D. L.; Arias Chavez, L. H.; Ben-Sasson, M.; Romero-Vargas Castrillón, S.; Yip, N. Y.; Elimelech, M. Desalination and Reuse of High-Salinity Shale Gas Produced Water: Drivers, Technologies, and Future Directions. *Environ. Sci. Technol.* **2013**, *47*, 9569−9583.

(5) Tanudjaja, H. J.; Hejase, C. A.; Tarabara, V. V.; Fane, A. G.; Chew, J. W. Membrane-based separation for oily wastewater: A practical perspective. *Water Res.* **2019**, *156*, 347−365.

(6) Bacchin, P.; Aimar, P.; Field, R. Critical and sustainable fluxes: Theory, experiments and applications. *J. Membr. Sci.* **2006**, *281*, 42−69.

(7) Wang, S.; Guillen, G.; Hoek, E. M. V. Direct Observation of Microbial Adhesion to Membranes. *Environ. Sci. Technol.* **2005**, *39*, 6461−6469.

(8) Zhu, Y.; Wang, D.; Jiang, L.; Jin, J. Recent progress in developing advanced membranes for emulsified oil/water separation. *NPG Asia Mater.* **2014**, *6*, No. e101.

(9) Tummons, E. N.; Tarabara, V. V.; Chew, J. W.; Fane, A. G. Behavior of oil droplets at the membrane surface during crossflow microfiltration of oil−water emulsions. *J. Membr. Sci.* **2016**, *500*, 211−224.

(10) Fux, G.; Ramon, G. Z. Microscale Dynamics of Oil Droplets at a Membrane Surface: Deformation, Reversibility, and Implications for Fouling. *Environ. Sci. Technol.* **2017**, *51*, 13842−13849.

(11) Tummons, E. N.; Chew, J. W.; Fane, A. G.; Tarabara, V. V. Ultrafiltration of saline oil-in-water emulsions stabilized by an anionic surfactant: Effect of surfactant concentration and divalent counter-ions. *J. Membr. Sci.* **2017**, *537*, 384−395.

(12) Tanudjaja, H. J.; Chew, J. W. Assessment of oil fouling by oil-membrane interaction energy analysis. *J. Membr. Sci.* **2018**, *560*, 21−29.

(13) Tanudjaja, H. J.; Chew, J. W. Critical flux and fouling mechanism in cross flow microfiltration of oil emulsion: Effect of viscosity and bidispersity. *Sep. Purif. Technol.* **2019**, *212*, 684−691.

(14) Ramon, G. Z.; Huppert, H. E.; Lister, J. R.; Stone, H. A. On the hydrodynamic interaction between a particle and a permeable surface. *Phys. Fluids* **2013**, *25*, 073103.

(15) Ramon, G. Z.; Hoek, E. M. V. On the enhanced drag force induced by permeation through a filtration membrane. *J. Membr. Sci.* **2012**, *392*−*393*, 1−8.

(16) Oron, A.; Davis, S. H.; Bankoff, S. G. Long-scale evolution of thin liquid films. *Rev. Mod. Phys.* **1997**, *69*, 931.

(17) Manor, O.; Vakarelski, I. U.; Tang, X.; O'Shea, S. J.; Stevens, G. W.; Grieser, F.; Dagastine, R. R.; Chan, D. Y. C. Hydrodynamic Boundary Conditions and Dynamic Forces between Bubbles and Surfaces. *Phys. Rev. Lett.* **2008**, *101*, 024501.

(18) Manor, O.; Vakarelski, I. U.; Stevens, G. W.; Grieser, F.; Dagastine, R. R.; Chan, D. Y. C. Dynamic Forces between Bubbles and Surfaces and Hydrodynamic Boundary Conditions. *Langmuir* **2008**, *24*, 11533−11543.

(19) Israelachvili, J. *Intermolecular and Surface Forces*; Elsevier Science, 2011.

(20) Tabor, R. F.; Wu, C.; Lockie, H.; Manica, R.; Chan, D. Y. C.; Grieser, F.; Dagastine, R. R. Homo- and hetero-interactions between air bubbles and oil droplets measured by atomic force microscopy. *Soft Matter* **2011**, *7*, 8977−8983.

(21) Chan, D. Y. C.; Klaseboer, E.; Manica, R. Theory of non-equilibrium force measurements involving deformable drops and bubbles. *Adv. Colloid Interface Sci.* **2011**, *165*, 70−90.

(22) Yiantsios, S. G.; Davis, R. H. On the buoyancy-driven motion of a drop towards a rigid surface or a deformable interface. *J. Fluid Mech.* **1990**, *217*, 547−573.

(23) Tabor, R. F.; Grieser, F.; Dagastine, R. R.; Chan, D. Y. C. Measurement and analysis of forces in bubble and droplet systems using AFM. *J. Colloid Interface Sci.* **2012**, *371*, 1−14.

(24) Doedel, E.; Keller, H. B.; Kernevez, J. P. Numerical Analysis and Control of Bifurcation Problems (I): Bifurcation in Finite Dimensions. *Int. J. Bifurcation Chaos* **1991**, *01*, 493−520.

(25) Dijkstra, H. A.; Wubs, F. W.; Cliffe, A. K.; Doedel, E.; Dragomirescu, I. F.; Eckhardt, B.; Gelfgat, A. Y.; Hazel, A. L.; Lucarini, V.; Salinger, A. G.; Phipps, E. T.; Sanchez-Umbria, J.; Schuttelaars, H.; Tuckerman, L. S.; Thiele, U. Numerical Bifurcation Methods and their Application to Fluid Dynamics: Analysis beyond Simulation. *Commun. Comput. Phys.* **2014**, *15*, 1−45.